Supplemental Material for "Predictions and Measurements of Thermal Conductivity of Ceramic Materials at High Temperature"

Zherui Han,[1,*] Zixin Xiong,[1,*] William T. Riffe,[2] Hunter B. Schonfeld,[3] Mauricio Segovia,[1] Jiawei Song,[4] Haiyan Wang,[4] Xianfan Xu,[1] Patrick E. Hopkins,[3,2,5] Amy Marconnet,[1,†] and Xiulin Ruan[1,‡]

[1]*School of Mechanical Engineering and the Birck Nanotechnology Center, Purdue University, West Lafayette, Indiana 47907-2088, USA*

[2]*Department of Materials Science and Engineering, University of Virginia, Charlottesville, Virginia 22904, USA*

[3]*Department of Mechanical and Aerospace Engineering, University of Virginia, Charlottesville, Virginia 22904, USA*

[4]*School of Materials Engineering, Purdue University, West Lafayette, Indiana 47907-2088, USA*

[5]*Department of Physics, University of Virginia, Charlottesville, Virginia 22904, USA*

(Dated: November 3, 2023)

CONTENTS

* These authors contributed equally to this work.

† marconnet@purdue.edu

‡ ruan@purdue.edu

Sec.1. FIRST-PRINCIPLES CALCULATIONS

All calculations are done using Density Functional Theory (DFT), Density Functional Perturbation Theory (DFPT) or *ab initio* molecular dynamics (AIMD) as implemented in the VASP package [1]. The first-principles settings for two ceramics are summarized in the table below:

Materials	XC functional	Optimization k-grid	Convergence criterion / (eV/Å)
CeO_2	LDA+U, $U_{\text{eff}} = 10$ eV [2, 3]	MK $12 \times 12 \times 12$	10^{-6}
MgO	PBE [4]	Γ-centered $11 \times 11 \times 11$	10^{-7}

Energy cutoffs for both materials are 520 eV. Born effective charges are computed by DFPT and with the aid of Phonopy [5] we get (1) for CeO_2: $\epsilon_\infty = 5.927$ (experiment gives 5.31 [6]), $Z^*_{Ce,xx} = 5.502$ and $Z^*_{O,xx} = -2.751$; (2) for MgO: $\epsilon_\infty = 3.241$ (experiment gives 2.96 [7]), $Z^*_{Mg,xx} = 1.980$ and $Z^*_{O,xx} = -1.980$.

Ab initio molecular dynamics are performed on a supercell structure consisting of 192 atoms constructed by $4 \times 4 \times 4$ CeO_2 primitive cells or 128 atoms of $4 \times 4 \times 4$ MgO primitive cells. Only the Γ point is computed to accelerate the calculation. After reaching thermal equilibrium under NPT ensemble (zero external pressure) with Langevin thermostat, we use 1000 more steps to get averaged lattice structure at each temperature. Then, on relaxed structure we perform NVT ensemble simulations and after reaching equilibrium we use 2000 more steps to construct effective force constants [8] at a time step of 2 fs. In the evaluation of force constants, cutoff radii are summarized in the table below:

Materials	Φ^*_2 cutoff / Å	Φ^*_3 cutoff / Å	Φ^*_4 cutoff / Å
CeO_2	6.31 Å	6 Å	4 Å
MgO	4.81 Å	4.5 Å	3.2 Å

Sec.2. QUANTUM CORRECTION TO MD TEMPERATURE

Our AIMD simulations suffer from incorrect statistics inherently seen in MD temperature. This would cause the thermal expansion to be always linear for materials with high Debye temperatures like MgO in our case. To partially overcome the limits of MD and connect

classical MD temperature T_{MD} with quantum temperature T, we have followed the treatment in [9] to correlate these two temperatures:

$$T_{MD} = \frac{2T^3}{{T_D}^2} \int_0^{T_D/T} \frac{x^2}{e^x - 1}\, \mathrm{d}x, \tag{S.1}$$

where T_D is the Debye temperature of a material.

Sec.3. NORMAL AND UMKLAPP FOUR-PHONON SCATTERING STRENGTH

We use RTA treatment of 4ph scattering when calculating κ. The effect of fully iterative solution with both 3ph and 4ph can be partially inferred from the relative importance of normal and Umklapp scattering in a certain material. The following figure (Fig. S1) shows the relative importance of N/U processes in the materials we simulated. Past theoretical investigations [10, 11] established an understanding that normal processes need to be dominant to have strong impact on thermal conductivity. It was shown that considering fully iterative solution in the case where N/U processes are just comparable gives underprediction of thermal conductivity by 3.5% - 7.5%. Based on this, we expect that RTA for 4ph channel would lead to computational error of κ than 10%.

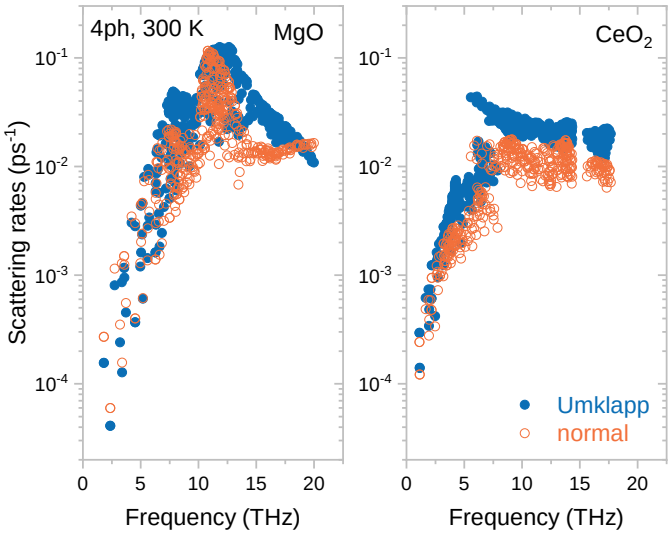

FIG. S1. Room temperature 4ph scattering rates in two materials decomposed into normal and Umklapp processes. Blue filled circles represent Umklapp processes and orange hallow circles represent normal processes.

Sec.4. VALIDITY OF PHONON GAS MODEL IN OUR SIMULATIONS

Our theory is based on phonon gas model. The phonon gas model is not applicable to cases where phonons cannot be well-defined in some crystals or at extreme conditions. Past theoretical works have attempted to resolve this challenge by using the concept of diffusons [12] or a dual-channel transport model [13]. Our approach is different in the sense that phonon renormalization scheme defines renormalized energies and scattering rates at high temperatures, preserving the concept of phonons. In our simulations of ceramic materials (MgO for instances), the majority of renormalized phonons do have mean free paths (MFPs) longer than interatomic distance (approximately 0.2 nm for MgO) even at 1500 K as shown in Fig. S2. Very few phonon modes (marked in red) have MFPs shorter than the interatomic distance and may be ill-defined. Since these modes have strong scattering rates, we expect them not to contribute much to thermal conductivity.

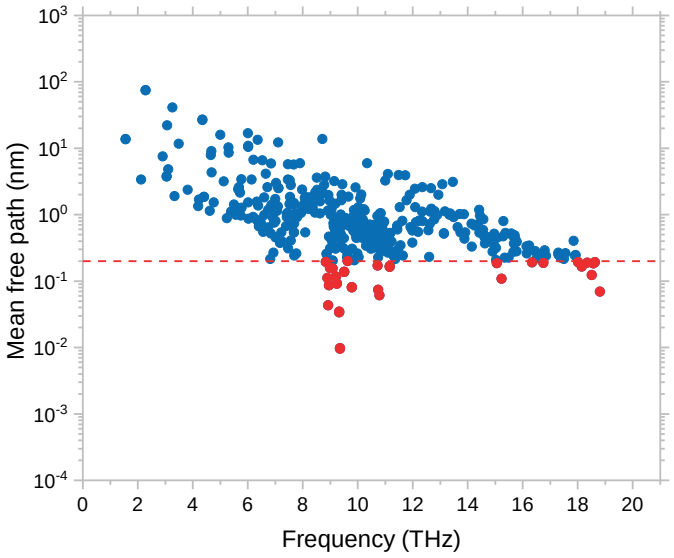

FIG. S2. Phonon mean free path of MgO at 1500 K as a function of phonon frequency. Red dots represent phonons whose mean free paths are shorter than 0.2 nm (red dashed line), the average interatomic distance of MgO crystal.

Sec.5. LOGARITHM PLOT OF TEMPERATURE-DEPENDENT THERMAL CONDUCTIVITY

Double-logarithm plot can better show power laws compared to normal plot in the main text. The following figure includes the same data from Fig. 6 of the main text but plotted in logarithm axes. It is clearly seen that power laws of κ incorporating 4ph scattering are affected by phonon renormalization for both materials.

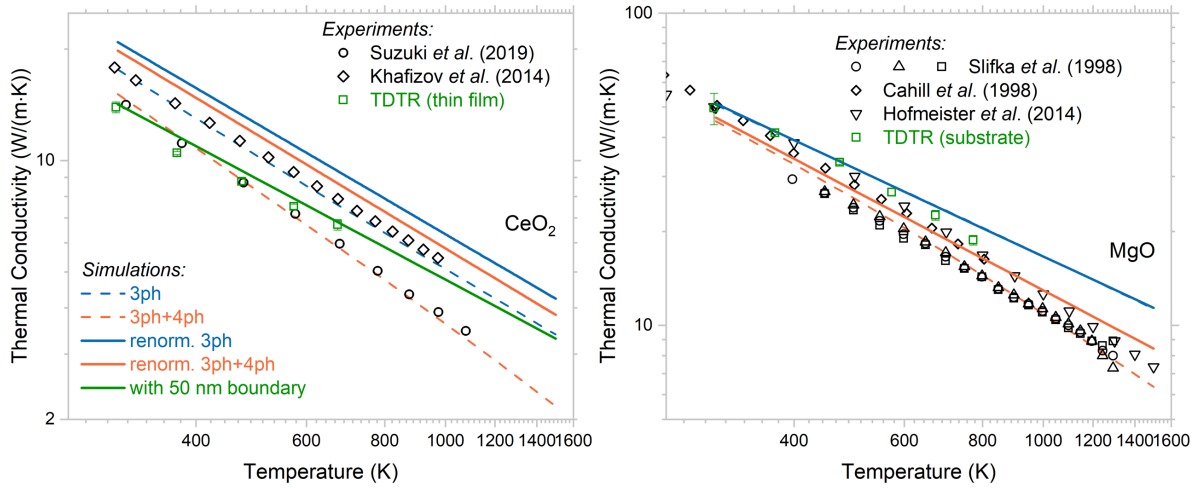

FIG. S3. Logarithm plot of Fig. 6 of the main text.

Sec.6. TDTR SENSITIVITY OF MGO AND CEO_2 ON STO SAMPLES

The sensitivity of the TDTR signal to a parameter α using magnitude and ratio analysis is calculated using the expressions:

$$S_\alpha = \frac{d \ln \sqrt{V_{in}^2 + V_{out}^2}}{d \ln \alpha}, \tag{S.2}$$

$$S_\alpha = \frac{d \ln \frac{V_{in}}{V_{out}}}{d \ln \alpha}. \tag{S.3}$$

Sensitivities to selected parameters for MgO substrate and CeO_2 film on STO substrate are plotted in Fig. S4. The sensitivity value at zero indicates the signal is independent of the parameter. On the other hand, the signal strongly depends on parameters with large sensitivity values. For both samples, the thermal conductivity of the material of interest has

high sensitivity. Therefore, the fitted thermal conductivities of MgO and CeO_2 have small uncertainties.

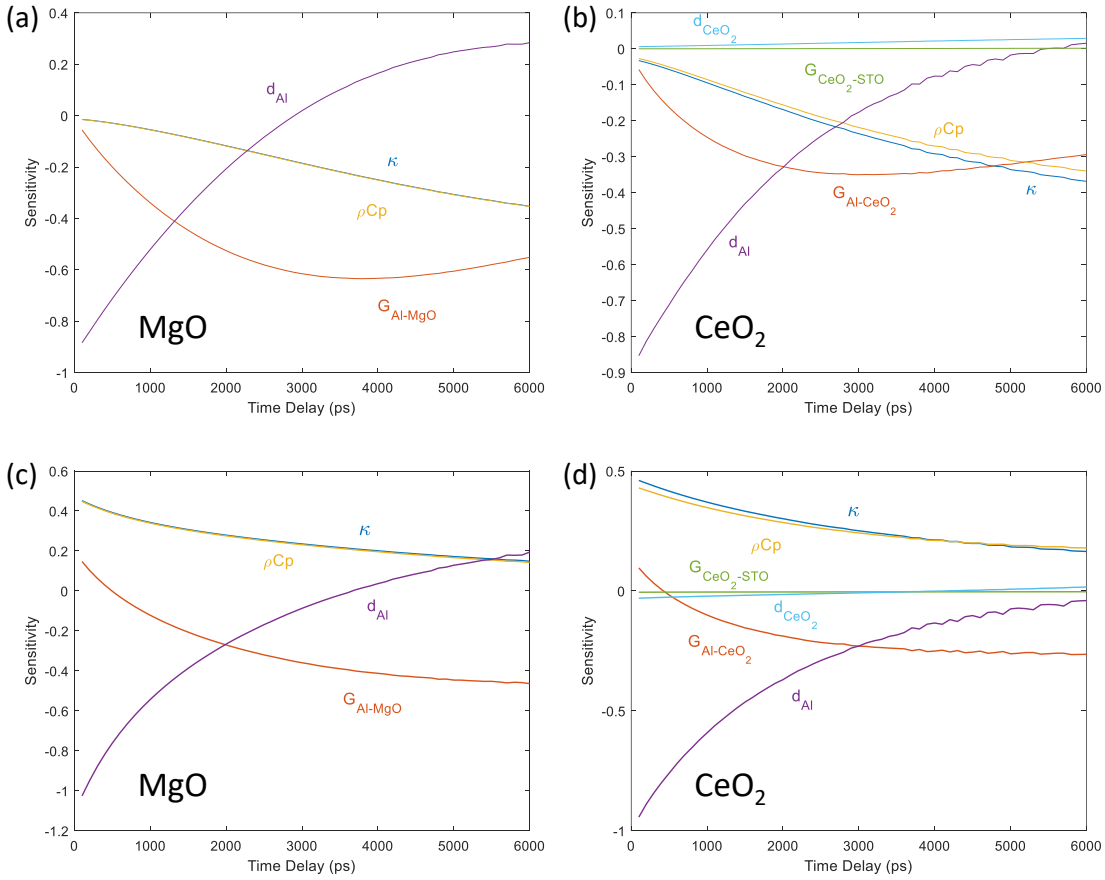

FIG. S4. The sensitivity of TDTR signal to selected parameters in MgO substrate and CeO_2 film on STO substrate samples using (a,b)magnitude and (c,d)ratio fitting methods. A larger absolute value of the sensitivity corresponds to higher sensitivity to a parameter. Parameter G_{X-Y} is the interface thermal conductance between material X and Y. Parameter d_X is the thickness of the material X.

Sec.7. TDTR MEASUREMENTS OF CEO_2 SUBSTRATE

Due to its low purity level, the purchased CeO_2 substrate shows low thermal conductivity as measured by TDTR method (Fig. S5). The measured temperature dependent thermal conductivity is similar to that of a CeO_2 pellet with 98% purity and 95% theoretical den-

sity [14, 15].

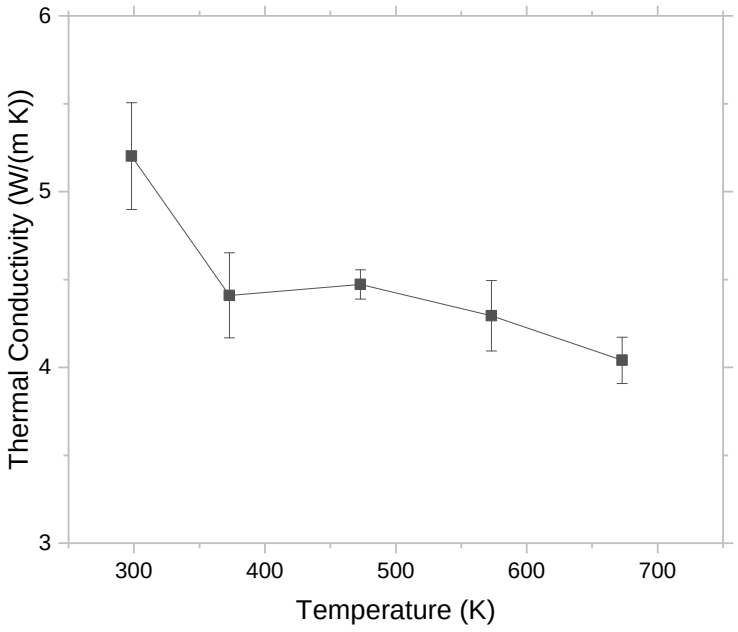

FIG. S5. The measured temperature-dependent thermal conductivity of a commercially available CeO_2 substrate. Low thermal conductivity is likely caused by low purity, which is estimated at 98% by comparing with data from literature [14].

Sec.8. GRAIN SIZE ESTIMATION BASED ON XRD

To characterize the crystallinity of the CeO_2 substrate, XRD (Panalytical X'Pert X-ray Diffractometer with Cu Kα1 (λ=0.154 nm) radiation source) was conducted. The crystallite size of the PLD-grown CeO_2 film is estimated using the Scherrer Equation:

$$d = \frac{k\lambda}{\beta cos\theta}, \tag{S.4}$$

where d is the average crystallite size, k is a constant with variable magnitude depending on geometry of the crystallite, λ is the wavelength of the X-ray, β is the full-width half-maxima of the XRD signal peak, and θ is the diffraction angle of the where the peak exists. Figure. S6 shows the XRD result of CeO_2 film on STO substrate. The estimated crystallite size is between 40 nm to 65 nm, based on which the boundary scattering is calculated. The

resolution of the XRD setup is 0.01 degree, resulting in an uncertainty in the calculated average grain size of 0.01 nm which is much less significant than the uncertainty due to peaks at different diffraction angles.

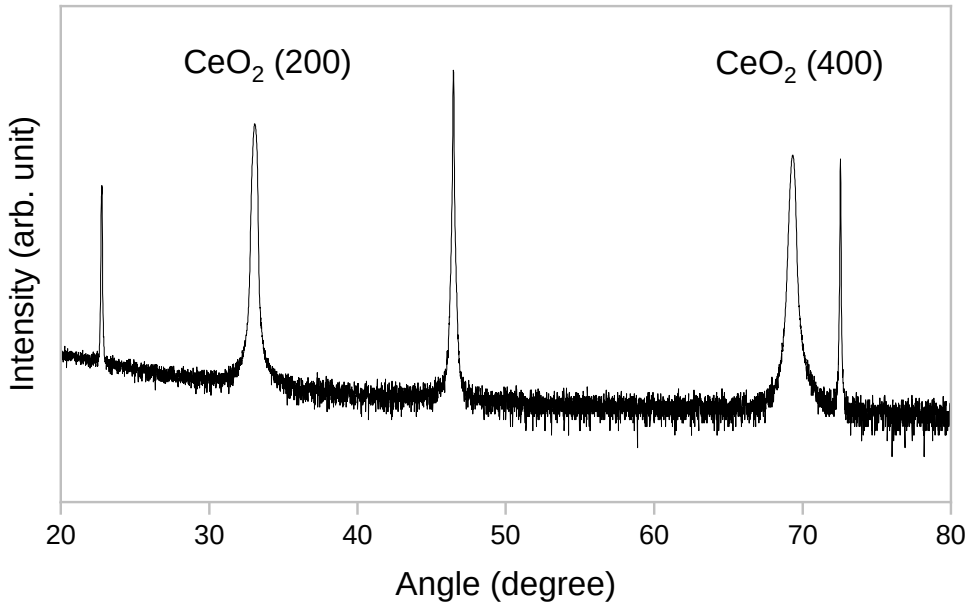

FIG. S6. The XRD result of PLD-grown CeO_2 film on STO substrate.

Sec.9. SAMPLE PREPARATIONS AND CHARACTERIZATIONS

The CeO_2 thin film was grown on STO (001) substrate, using a pulsed laser deposition (PLD) technique with a KrF excimer laser (Lambda Physik, $\lambda = 248$ nm, 10 Hz). Before deposition, the chamber was pumped to vacuum ($< 1 \times 10^{-6}$ Torr), and substrate temperature was kept at 600 °C. A 20 mTorr oxygen pressure was used during deposition and the chamber was naturally cooled down to room temperature at 20 mTorr oxygen partial pressure after deposition. The Energy Dispersive Spectroscopy (EDS) mapping of the PLD grown CeO_2 film shows the atomic fraction of Ce and O are 28.47±4.66% and 71.53±8.29%, respectively. Based on the Ce and O composition in the EDX data, it suggests the CeO_2 thin film is close to stoichiometry. The higher oxygen content than expected (33% Ce, 66%

O) in the EDX data is due to the surface oxygen contamination on the TEM specimen foil.

---

[1] G. Kresse and J. Hafner, Ab initio molecular dynamics for liquid metals, Phys. Rev. B **47**, 558 (1993).

[2] V. I. Anisimov, J. Zaanen, and O. K. Andersen, Band theory and mott insulators: Hubbard u instead of stoner i, Phys. Rev. B **44**, 943 (1991).

[3] C. Loschen, J. Carrasco, K. M. Neyman, and F. Illas, First-principles LDA+U and GGA+U study of cerium oxides: Dependence on the effective U parameter, Phys. Rev. B **75**, 035115 (2007).

[4] J. P. Perdew, K. Burke, and M. Ernzerhof, Generalized Gradient Approximation Made Simple, Physical Review Letters **77**, 3865 (1996).

[5] A. Togo and I. Tanaka, First principles phonon calculations in materials science, Scr. Mater. **108**, 1 (2015).

[6] S. Mochizuki, Infrared optical properties of cerium dioxide, physica status solidi (b) **114**, 189 (1982).

[7] E. Calandrini, L. Paulatto, D. Antonangeli, F. He, R. P. S. M. Lobo, F. Capitani, J.-B. Brubach, P. Roy, L. Vincent, and P. Giura, Limits of the quasiharmonic approximation in MgO: Volume dependence of optical modes investigated by infrared reflectivity and ab initio calculations, Physical Review B **103**, 054302 (2021).

[8] O. Hellman and I. A. Abrikosov, Temperature-dependent effective third-order interatomic force constants from first principles, Phys. Rev. B **88**, 144301 (2013).

[9] J. Hu, X. Ruan, and Y. P. Chen, Thermal Conductivity and Thermal Rectification in Graphene Nanoribbons: A Molecular Dynamics Study, Nano Letters **9**, 2730 (2009).

[10] T. Feng, L. Lindsay, and X. Ruan, Four-phonon scattering significantly reduces intrinsic thermal conductivity of solids, Phys. Rev. B **96**, 161201(R) (2017).

[11] N. K. Ravichandran and D. Broido, Unified first-principles theory of thermal properties of insulators, Phys. Rev. B **98**, 085205 (2018).

[12] M. T. Agne, R. Hanus, and G. J. Snyder, Minimum thermal conductivity in the context of diffuson-mediated thermal transport, Energy & Environmental Science **11**, 609 (2018).

[13] Y. Luo, X. Yang, T. Feng, J. Wang, and X. Ruan, Vibrational hierarchy leads to dual-phonon transport in low thermal conductivity crystals, Nature Communications **11** (2020).

[14] A. T. Nelson, D. R. Rittman, J. T. White, J. T. Dunwoody, M. Kato, and K. J. McClellan, An Evaluation of the Thermophysical Properties of Stoichiometric CeO2 in Comparison to UO2 and PuO2, Journal of the American Ceramic Society **97**, 3652 (2014).

[15] K. Suzuki, M. Kato, T. Sunaoshi, H. Uno, U. Carvajal-Nunez, A. T. Nelson, and K. J. McClellan, Thermal and mechanical properties of CeO2, Journal of the American Ceramic Society **102**, 1994 (2019).